Mach Stem Formation in Outdoor Measurements of Acoustic Shocks

Kevin M. Leete

A senior thesis submitted to the faculty of

Brigham Young University

In partial fulfillment of the requirements for the degree of

Bachelor of Science

Dr. Kent L. Gee, Advisor

Dr. Tracianne B. Neilsen, Co-advisor

Department of Physics and Astronomy

Brigham Young University

April 2016

ABSTRACT

Mach Stem Formation in Outdoor Measurements of Acoustic Shocks

Kevin M. Leete

Department of Physics and Astronomy

Bachelor of Science

Mach stem formation in acoustic shocks is investigated using oxyacetylene balloon explosions conducted a short distance above pavement. As the shock wave propagates away from the blast site it transitions from a regular reflection to irregular reflection. The location of this transition point, as well as the path of the triple point, are experimentally resolved using microphone arrays and a high-speed camera. The measured transition point falls between that predicted from derivations based on weak shock waves and an empirical relationship derived from large-scale explosions. It also agrees well with predicted values based on von Neumann's three shock theory.

Table of Contents

List of Figures

Chapter 1

Introduction

1.1 Background

A shock wave is an acoustic wave that is characterized by having a nearly discontinuous jump in the acoustic variables of the medium. Ernst Mach was the first to investigate the reflection of shock waves in 1878.[1] From his original investigation, he observed two types of shock wave reflection: regular and irregular. The regular reflection of a shock wave consists of an incident shock and a reflected shock which intersect at the reflecting surface, whereas an irregular reflection consists of three shocks: the incident shock, reflected shock, and a third shock called a Mach stem that travels parallel to the surface. The intersection of these three shocks is called the triple point. The Mach stem is formed because the incident shock heats up the medium so the reflected shock can propagate slightly faster, which allows for the reflected shock to catch up to the incident shock and merge. Figure 1is an illustration of the two general types of reflection. The incident shock is obliquely impinging on a rigid surface, travelling from right to left. In

Panel a) the regularly reflected shock is shown coming off the rigid wall and travelling to the left as well. Panel b) shows the irregularly reflected shock meeting with the incident shock a short distance above the reflecting plane and the merged shock known as the Mach stem travelling parallel to the surface. The point at which the three shocks touch is known as the triple point. In some instances, there is a contact discontinuity or slipstream that trails off the triple point to separate the region of air that has travelled through the incident and reflected shocks from the air that only passed through the Mach stem.

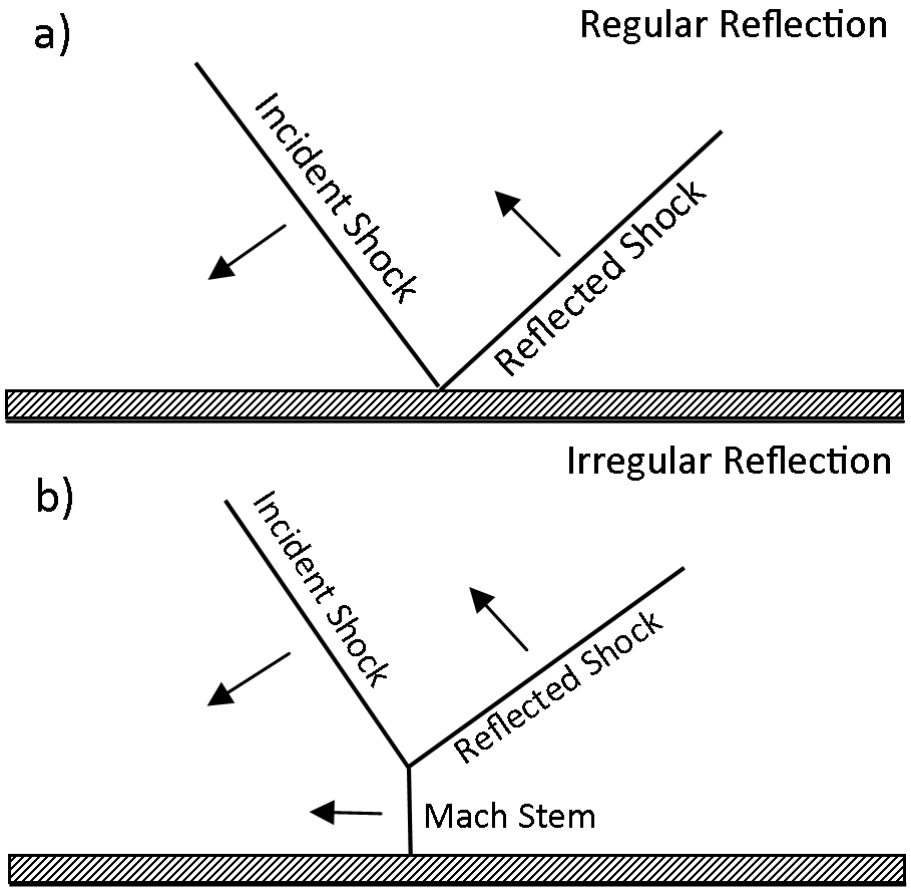

Figure 1 A schematic of the two general types of shock wave reflections with the incident shock propagating from the upper right to the lower left. Panel a) shows a regular reflection with the incident shock and reflected shock intersecting at a single point along the rigid surface. The incident and reflected angles are slightly different and are dependent on the amplitude of the incident shock. Panel b) shows an irregular reflection, the incident and reflected shocks join at a point above the reflecting surface (called the triple point) and a Mach stem connects the triple point to the reflecting surface.

Sixty- five years after Mach's investigation, John von Neumann thoroughly studied the phenomenon and created what is called "two-shock theory" and "three-shock theory".[2] The theories consist of taking the configuration of two or three straight shocks and applying the Rankine-Hugoniot jump conditions across each shock, jointly with the equation of state for each of the regions separated by the shocks. This sets up a system of nonlinear equations that may or may not have a physically-realizable solution. The system of equations can be reduced to two parameters such as the incident shock Mach number $M_s = v_s/c_0$ (the ratio of the velocity of the shock to the ambient sound speed) and incident angle ϕ (the angle measured from the velocity vector of the shock to the plane of the reflecting surface). One can determine which type of reflection can exist in each point in the M_s- ϕ space by which theory has physical solution. However, in many experimental studies it has been found that irregular reflections persist into regions where there is not a solution to the three shock theory, especially in regimes where $M_s < 1.47$.[3] This regime is known as the weak shock reflection domain, and the inconsistency with von Neumann's three shock theory is known as the von Neumann paradox.[4]

Ever since the discovery of the von Neumann paradox, shock wave reflections have been studied numerically and experimentally. Through innovation in experimental technology and numerical modeling, the von Neumann paradox has been resolved by finding that the actual configurations of shock wave reflection are not, in most cases, two or three straight shocks.[5,6] This has prompted the need for observation and classification of all the different types of reflections. Works such as Ben-dor's *Shock Wave Reflection Phenomena* (2007)[4] have put forth classification schemes, but since this topic is still an active area of research there is no standard nomenclature.

1.2 Previous Work

1.2.1 Theoretical

Semenov *et. al.*[7] seems to be the most up-to-date examination of the M_s and ϕ parameter space. He proposes a classification scheme for various types of reflections based on shapes of the reflected wave, Mach stem, and slipstream, as well as traces out regions on the M_s-ϕ plane where each type of reflection can occur. Figure 2 A graph of the different boundaries on the $\boldsymbol{\phi}$-$\boldsymbol{M_s}$ plane that separate regions of shock reflection types.as taken from Semenov *et al.*[7] The blue line marks the transition from regular to irregular reflection in classical two shock theory, and the others are added by Semenov. The regions are marked by the reflection type. RR for regular reflection, SM-SR for single Mach-Smith reflection. wSM-SR for weak single Mach-Smith reflection, and vNR for von Neumann reflection. The triangular region between the green, blue and purple lines is described as a region that has been completely ignored by research until this point.[7] is a portion of the M_s-ϕ plane in the region where $M_s < 1.5$ which contains the boundaries that separates regions of different shock reflection types.

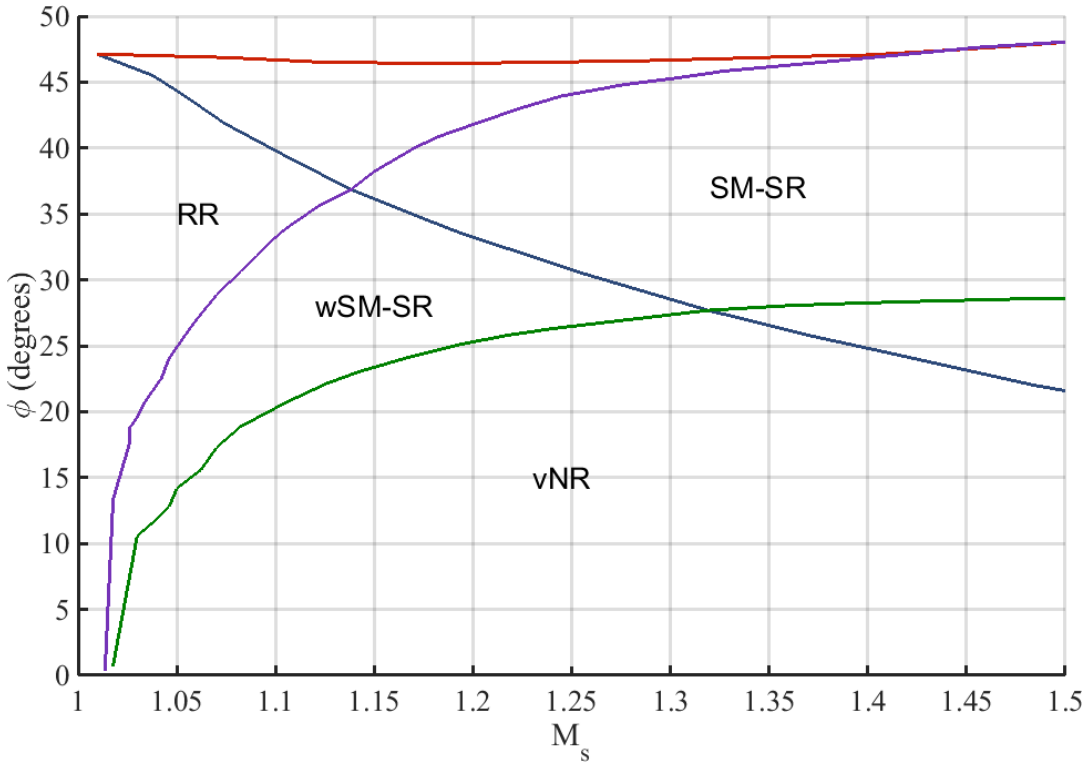

Figure 2 A graph of the different boundaries on the $\boldsymbol{\phi}$-$\boldsymbol{M_s}$ plane that separate regions of shock reflection types.as taken from Semenov *et al.*[7] The blue line marks the transition from regular to irregular reflection in classical two shock theory, and the others are added by Semenov. The regions are marked by the reflection type. RR for regular reflection, SM-SR for single Mach-Smith reflection. wSM-SR for weak single Mach-Smith reflection, and vNR for von Neumann reflection. The triangular region between the green, blue and purple lines is described as a region that has been completely ignored by research until this point.[7]

Three types of irregular reflection that could occur in this regime are the von Neumann reflection (vNR), Single Mach-Smith reflection (SM-SR), and weak single Mach-Smith reflection (wSM-SR). Although vNR and SM-SR both form a Mach stem, the interaction of weaker waves in the case of the von Neumann reflection results in a continuous slope between the Mach stem and incident shock wave at the triple point. SM-SRs, on the other hand, have a slope discontinuity between the incident shock and Mach stem at the triple point and a slipstream that trails behind the triple point trajectory. The difference between the single Mach-Smith reflection and the weak single Mach-Smith reflection is the angle between the incident and reflected shocks. These are summarized in Figure 3, which is based off of a figure from Ref [7].

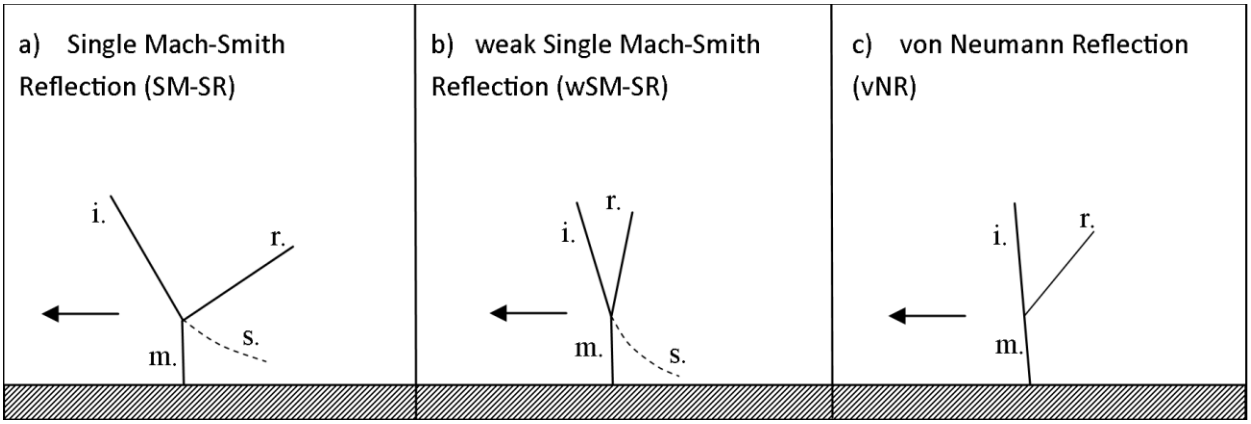

Figure 3 A schematic of three types of irregular reflections that could occur in the weak shock reflection regime. a) A Single Mach-Smith Reflection, characterized by an incident shock (i.), reflected shock (r.), a Mach stem (m.), and a slipstream (s.) that trails the path of the triple point. b) A weak Single Mach-Smith Reflection which is identical to a) except for the angle between the incident and reflected shocks. c) The von Neumann reflection is characterized by having a continuous slope between the Mach stem and the incident wave, a reflected shock that has degraded to either a simple compression wave or, in some cases, and expansion fan.

1.2.2 Experimental

Each point in the M_s-ϕ plane represents a solution to the shock reflection problem that can be experimentally tested by using shock tubes. A shock tube is a long tube with a thin membrane that separates high and low pressure states. The membrane is then ruptured, causing an approximate step shock to propagate down the tube. If a rigid wedge is placed in the tube, the wedge angle acts as the incident angle of the shock. In a shock tube, the flow can be described as "pseudo-steady", because within reasonable approximation the shock does not lose amplitude as it propagates. In this way a single point on the M_s- ϕ plane can be probed.

The irregular reflection of spherical unsteady shocks, such as those generated by a point explosion, is more complex because the amplitude of the shock and the angle of incidence, ϕ, both decrease with distance. Figure 4 Illustrative example of the difference between a shock tube experiment and a point explosion above a reflecting surface. a) a point explosion above a rigid

surface has a shock whose incident angle decreases as it propagates outward. b) a shock produced in a shock tube with a rigid wedge has an incident angle that is constant throughout the experiment schematically shows the difference between a shock tube experiment and an explosion over a rigid surface.

Decreasing the amplitude of the shock discourages irregular reflection, while approaching grazing incidence encourages it. For the case of an explosion over a rigid surface, regular reflection Generally occurs close to the source, and as the shock propagates outward it transitions to irregular reflection. Although there are no canonical analytic solutions for the transition point from regular to irregular reflection, various approaches have been employed. The most common method is to analyze the shock process for each individual point along the reflecting surface, calculating the incident angle and Mach number and tracing a curve on the M_s-ϕ plane. The intersection of the traced path of the reflection parameters with a boundary line between two reflection regimes is then deemed the transition point.[4] However, the validity of this method is in question because of observed hysteresis effects, where a propagating shock tends to stay in its current configuration until it is further into the next regime.[8]

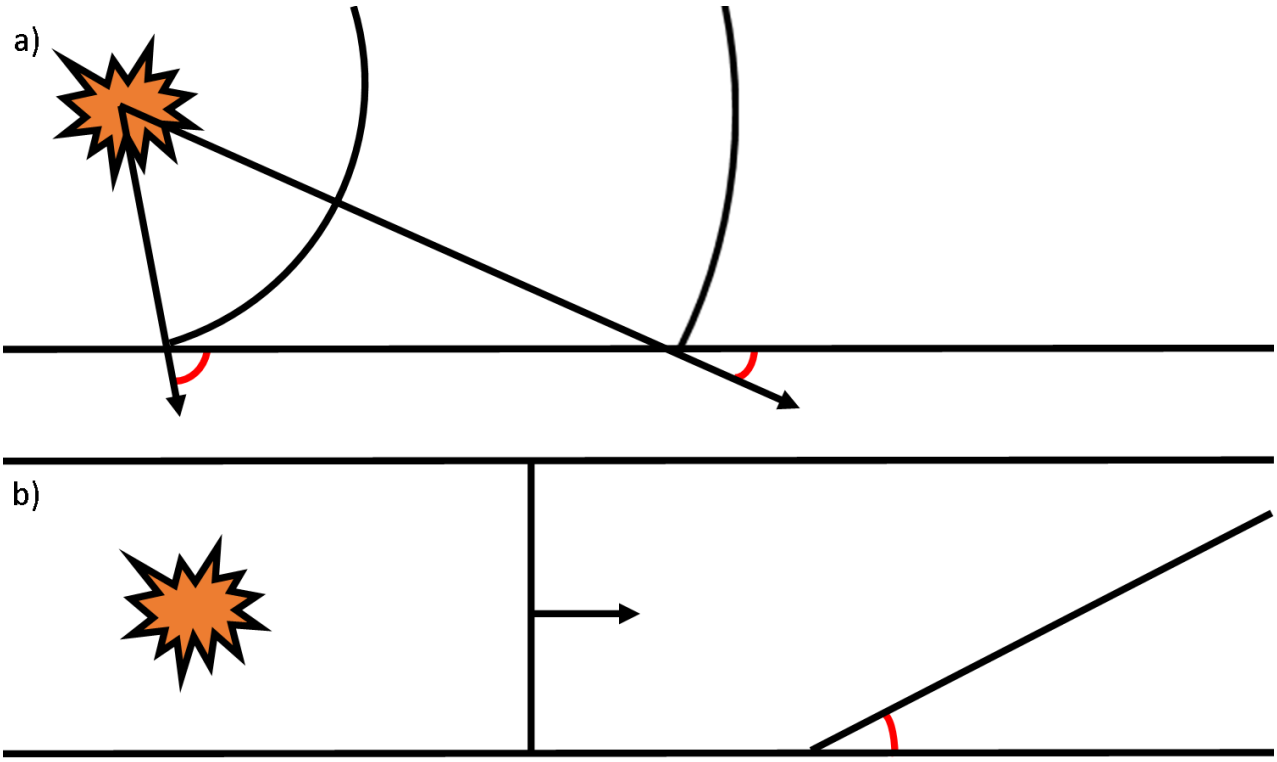

Figure 4 Illustrative example of the difference between a shock tube experiment and a point explosion above a reflecting surface. a) a point explosion above a rigid surface has a shock whose incident angle decreases as it propagates outward. b) a shock produced in a shock tube with a rigid wedge has an incident angle that is constant throughout the experiment

1.2.3 Theory for an unsteady shock

A solution to the problem of an unsteady spherical shock reflected over a rigid surface was recently derived by Baskar et al.[9] They introduced a critical parameter derived from the nonlinear Khokhlov-Zabolotskaya-Kuznetsov equations to describe the transition of a shock from regular to different types of irregular reflection. The critical parameter, called a, is calculated by

$$a = \frac{\sin(\phi)}{\sqrt{2\beta M_a}}, \tag{1}$$

where $M_a = \Delta P/(\gamma P_0)$ is the peak acoustic Mach number of the waveform, ΔP is the pressure change across the shock, γ is the ratio of specific heats, P_0 is the ambient pressure, and β is the coefficient of nonlinearity of the medium. M_a can be related to the shock Mach number, M_s, by the peak pressure value of the shock. Since a is then a function of both M_s and ϕ, it can be compared to existing transition lines by plotting contours of the parameter on the M_s-ϕ plane. Their assertion is that the transition from regular reflection to von Neumann type reflection occurs at the contour $a = 0.8$. However, in experimental tests, Karzova et al.[10] found for weak shocks generated by spark-pulses ($M_a < 0.01$) the transition point did not compare with those predicted by a for all cases; they found that the transition from regular to irregular reflection to be along the $a = 1.1$ contour. Figure 5 is Figure 2 with these two parameter a contours overlaid.

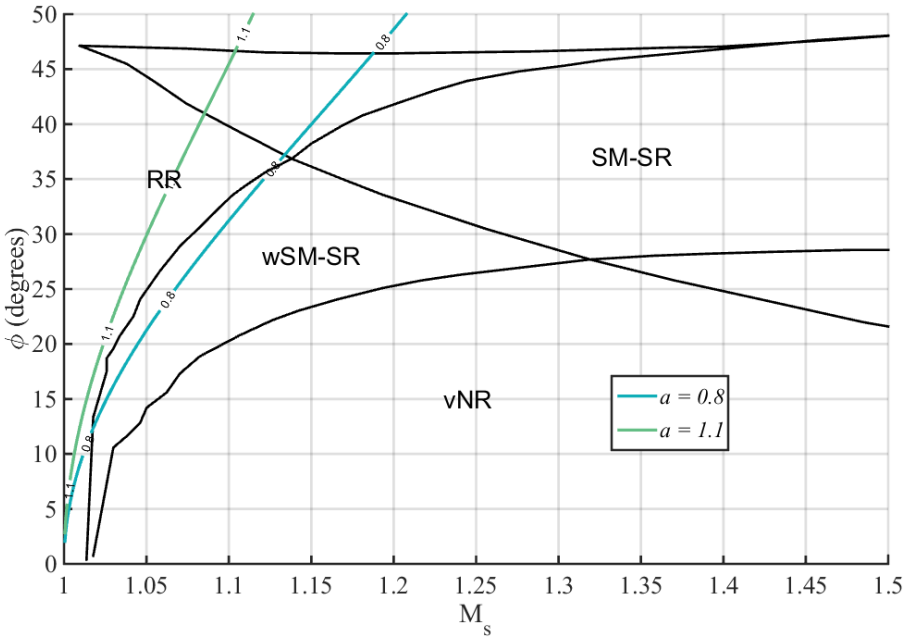

Figure 5 $\boldsymbol{M_s}$-$\boldsymbol{\phi}$ plane with the parameter $\boldsymbol{a}$ contours overlaid. It can be seen that for very small shock Mach numbers the parameter $\boldsymbol{a}$ contours seem to coincide with the transition from regular to irregular reflection given by

Semenov *et al*. However, the $\boldsymbol{a = 0.8}$ contour starts to deviate drastically starting at about $\boldsymbol{M_s = 1.15}$, with the $\boldsymbol{a = 1.1}$ contour deviating even earlier.

The two contours of this parameter seem to converge as M_s becomes very small, and they both tend to follow the line which Semenov[7] claims to be the transition from RR to SM-SR.

1.2.3 Empirical solutions

Finally, to solve for the transition point from regular to irregular reflection without analytics, empirical fits[11,12] to data from large explosions allow the calculation of Mach stem formation distance, triple point height, and stem overpressure as functions of height-of-burst (HOB) and equivalent yield in kilotons of TNT (kt TNT). However, given the disparity in scales, the validity of applying these fits which were made to large scale explosions to small-scale explosions approaching the acoustical weak-shock regime is in question.

1.3 Scope of Thesis

In this thesis, I study the weak shock reflection regime by exploding oxyacetylene balloons a short distance above pavement. The peak acoustic Mach numbers of the shocks ranged from $0.02 < M_a < 0.5$ and shock Mach numbers from $1.01 < M_s < 1.3$ at the points of reflection across the angular range $6° < \phi < 48°$. The shock propagation and reflection are well documented by acoustic transducers and a high speed camera. Comparisons of this data are made against the equivalent HOB empirical fits based on higher-amplitude explosions, the parameter a, which was derived for lower-amplitude shocks, and by tracing out the evolution in

M_s-ϕ plane. The transition from regular to irregular reflection was observed and a tentative classification for the irregular reflection type is made.

Chapter 2

Experiment

This Chapter outlines the experiment which was conducted in April of 2015 as well as how the acoustic and video data was processed as well as a summary of the data

2.1 Setup

Recent studies have shown that spherical oxyacetylene balloons are reliable sources of weak shock waves[13] and identified the presence of irregular reflections in outdoor measurements.[14] To use this to measure irregular reflection of shack waves an experiment was conducted in April of 2015 where we took large, spherical balloons filled with a stoiciometrically balanced mix of acetylene and oxygen and exploded them a short distance above pavement in a large, open area. The current experiment, shown in Figure 6, is similar to the one conducted in Ref [14], except with the oxyacetylene balloon placed closer to the ground so that irregular reflections are

triggered closer to the source. The 0.685 m diameter balloons were placed in a tripod-mounted metal cradle with the balloon center 1.8 m off the ground and the propagation of the shock waves were measured along an 18 m line. The x axis is defined as the horizontal range along the propagation line from the point directly below the balloon, and the z axis is the height above the pavement.

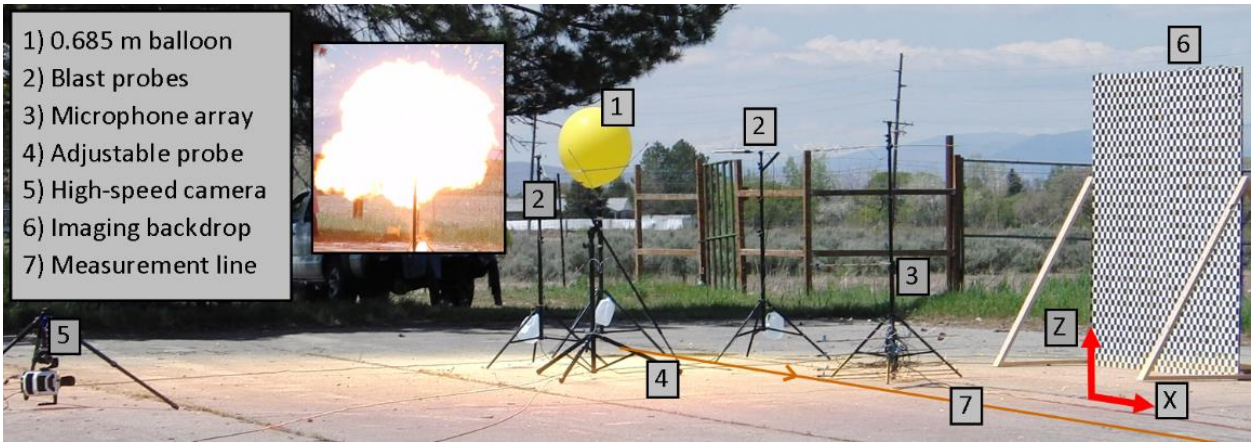

Figure 6 Mach-stem experiment setup with 1) gas-filled balloon in its metal cradle at z = 1.8 m; 2) two reference pressure gauges at 1.35 and 1.27 m; 3) vertical array of GRAS pressure microphones; 4) pressure probe attached to adjustable boom arm; 5) Phantom high-speed camera; 6) high-contrast checkerboard backdrop; 7) Line of propagation (x-axis). (Inset) balloon explosion.

A model rocket igniter was taped to the balloon and connected to a long BNC cable, which was connected to an ignition switch to allow for detonation at a safe distance. Two PCB pressure probes (models 112A23 and 137B24B) to be used as references were located on tripods at fixed distances (1.35 m and 1.27 m) about 45° on either side of the x axis. Over the 25 detonations, the standard deviation in peak SPL measured at these reference probes were 0.35 dB and 0.50 dB respectively. A tripod with an array of GRAS 6.35 mm, 46BG pressure microphones attached at $z = 0.03$, 0.05, 0.10, 0.20, 0.30, 0.91, and 1.83 m was placed at 15 different locations in x throughout the test, to scan the length of the propagation line. An additional PCB 112A23 probe

was attached to the end of a tripod with an adjustable boom arm to provide additional resolution at areas of interest. To minimize scattering, all probes and microphones were taped to the end of 9.5 mm diameter wooden dowels which extended horizontally from the tripods.

Pressure waveforms were recorded using a system comprised of National Instruments PXI-4462 dynamic signal acquisition devices with a sampling frequency of 204.8 kHz. A Kestrel 4500BT weather meter was used to log the ambient temperatures, pressures, humidity, wind speed, and direction for each test. The ambient pressure used in calculations was relatively constant at 87 kPa during the experiments and the wind was low enough to be considered negligible.

Below is a table of the microphone positions for each of the 25 detonations. Left out values correspond to runs where there was either a misfire or the data acquisition system did not catch the shock wave.

Table 1 A table of values for the array distance and adjustable boom position for each explosion.

ID	Array distance	Adjustable boom position (x,z)	ID	Array distance	Adjustable boom position (x,z)
1	-	-	**14**	35’	17.5’,6”
2	10’	10’,2’	**15**	37.5’	20’,9”
3	10’	-	**16**	36.5’	20’,10”
4	15’	10’,1’	**17**	36’	20’,11”
5	15’	9’,1”	**18**	55’	22.5’,18”
6	17.5’	9’,3/4”	**19**	52.5’	22.5’,15”
7	17.5’	9’,1/2 ”	**20**	53.5’	30’,24”
8	25’	9’,1”	**21**	-	-
9	20’	12’,2”	**22**	54’	30’,25”
10	20’	12’,2”	**23**	54’	22.5’,13”
11	22.5’	12’,3”	**24**	54.5’	22.5’,14”
12	22.5’	12’,3”	**25**	54.5’	50’,44”
13	30’	17.5’,6”			

For safety, the oxygen and acetylene tanks were secured to the back of a pickup truck a reasonable distance from the detonation zone. We used a balanced mix of acetylene and oxygen to maximize combustion efficiency: first, the balloon was filled with acetylene to a diameter of 0.53 m then filled to its full diameter with oxygen. We constructed plastic rings of the appropriate diameters and filled the balloons until they fit snugly in the rings to ensure consistency. All handlers of the balloons were wearing flame retardant lab coats, eye protection and face masks. Everyone in proximity to the blast zone used double hearing protection.

To visualize the shockwave propagation, a Phantom v1610 high-speed camera operating at 18,002 frames per second recorded four separate regions along the propagation line for different explosions: $x =$ 3.35 to 5.79 m, 2.13 to 4.57 m, 6.10 to 8.53 m, 9.14 to 11.58 m. In these regions, a 2.4 x 2.4 m checkerboard backdrop was placed 3.05 m behind the propagation line to provide additional contrast for the camera.

2.2 Acoustic Data Processing

Each acoustic waveform needed to be looked at individually to determine its peak pressure. A representative waveform, shown in Figure **7**a), illustrates that there is a significant Gibbs phenomena present. The peak pressure was determined by extrapolating the downward slope of the shock to the shock front.

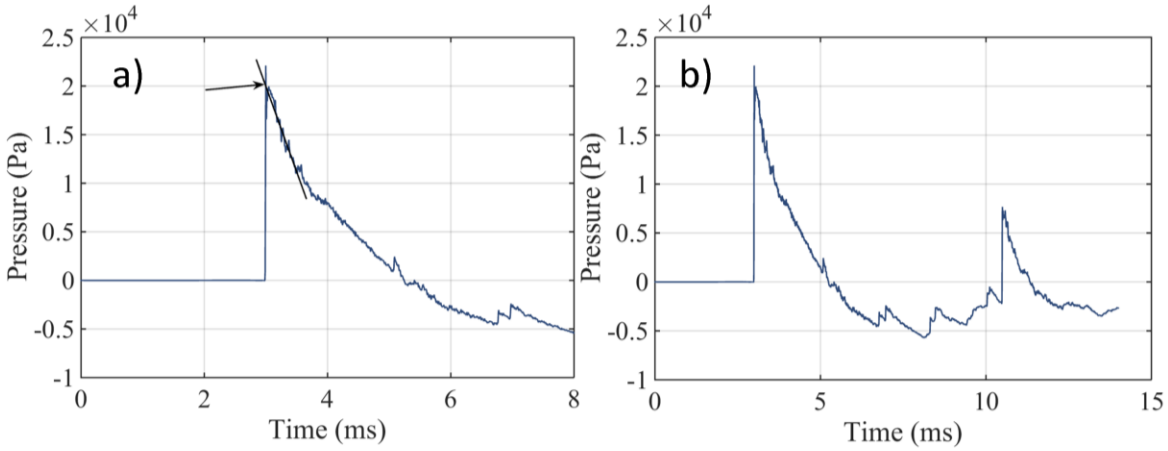

Figure 7 Example of method used to record peak amplitude and identify reflection type. A) the pressure waveform as a function of time contains a large Gibb's phenomena-like peak. To identify the peak pressure, a line was approximated to the slope of the decaying portion; the intersection of this line with the initial peak was called the peak pressure. b) a representative example of a waveform which obviously contains two shocks, an incident shock and a reflected shock. Therefore, at this microphone if an irregular reflection was occurring at this $\boldsymbol{x}$ value, the Mach stem passed below the microphone.

Whether regular or irregular reflection is occurring at the position of the microphone can be seen in the microphone data. For example, in Figure **7** Example of method used to record peak amplitude and identify reflection type. A) the pressure waveform as a function of time contains a large Gibb's phenomena-like peak. To identify the peak pressure, a line was approximated to the slope of the decaying portion; the intersection of this line with the initial peak was called the peak pressure. b) a representative example of a waveform which obviously contains two shocks, an incident shock and a reflected shock. Therefore, at this microphone if an irregular reflection was occurring at this $\boldsymbol{x}$ value, the Mach stem passed below the microphone.b), both an incident shock and a reflected shock are seen, therefore either a regular reflection is occurring at this point, or, if an irregular reflection were occurring, the triple point passed below the microphone.

With the peak pressure identified for each microphone position, we can now fit the pressure decay to a curve. A simple exponential function was used:

$$P_{peak} = Ar^B + C, \tag{2}$$

where A, B, and C are the fitted parameters and r is the radial distance (in feet) from the center of the balloon. The least squares fit determined the constants to be $A = 1.2 \times 10^6$, $B =$ -1.7, and $C = 1.1 \times 10^3$. These were only fit to points where the Mach stem had not formed, because the peak pressures of the Mach stem is larger than the combined incident and reflected waves.

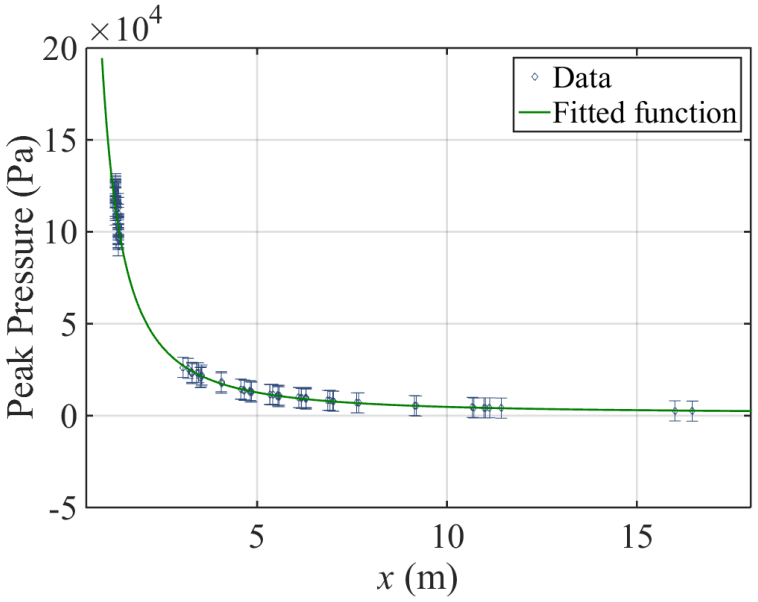

Figure 8 Peak pressure of the shock as a function of radial distance from the balloon center. Data were taken only from the peak pressure of the initial shock where it had not yet formed a Mach stem. The red line is the fitted function of the form $\boldsymbol{P_{peak} = Ar^B + C}$.

2.3 Visual Data Processing

The shock is visualized by subtracting two adjacent frames of the footage. These difference images were converted to grayscale and the resulting histograms readjusted such that pixels with

above a certain threshold value were saturated to white and all other values linearly distributed from black to white. To increase visibility, a color map varying from deep red to white was used.

Once the shock was visualized on the footage, a function to map the pixel position to the real position in space was needed. Calibration was achieved by placing the backdrop along the x axis at each camera location and taking a still picture. Knowing the width of the checkerboard pattern, one can count the number of pixels between lines and come up with a "pixels per inch" value. Then, the pixel where the backdrop contacts the concrete can be called $z = 0$. To calibrate the absolute position along the x-axis, a marker was placed along the propagation line at a known x value, and the horizontal pixel value of the can's position was recorded. With these anchors to real distances and a pixel per inch value, a function can be created to map a pixel value to real x and z values.

2.4 Triple Point Localization

2.4.1 Acoustic data

The spatial sampling of the acoustic data gives a more accurate representation of the position of the triple point, based on examining the waveform for the presence of one or two shocks. An illustrative example is given in Figure 9. Figure 9a) and 9c) show a single frame of the high-speed video with the locations of three 46BG microphones superimposed at x = 4.6 and 6.9 m respectively. Figures 9b) and 9d) show pressure waveform segments for the three microphones at the same locations. As seen in Figure 9b), at z = 0.10 m a single shock is present in the acoustic data, corroborated by the Mach stem passing through the image of Fig. 9a). Further, the

incident and reflected shocks are both present at $z = 0.20$ m and $z = 0.30$ m, which is verified by the two unmerged shocks of Fig. 9a). Consequently, the position of the triple point can be identified between z = 0.10 and 0.20 m. Figs. 9c) and 9d) show similar data, but at x = 6.9 m. At this distance, the image in Fig. 9c) has more uncertainty in the triple point position due to the lower signal strength. However, the acoustic data shown from two closely spaced microphones allow for the identification of the triple point location between $z = 0.36$ m and 0.38 m.

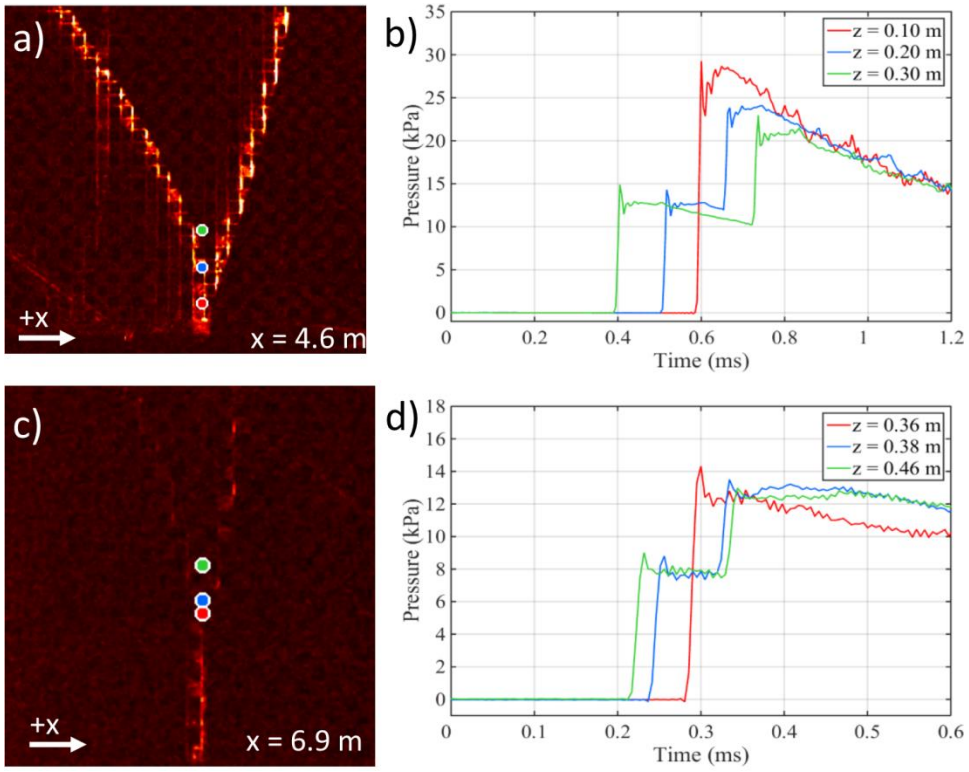

Figure 9 Two methods for identifying triple point location: 1) A single frame of high-speed video (a) showing the irregular reflection of a shock wave at x = 4.6 m downstream from the source. 2) A pressure vs. time graph (b) of three separate microphones located at different heights at x = 4.6 m with relevant positions superimposed as the colored dots on (a). (c) and (d) are similar images and pressure measurements at x = 6.9 m.

2.4.2 Visual Data

Attached with this thesis is a compilation of the processed high-speed video from the four regions along the propagation line as well as an explanatory introduction. Microphone positions as well as a cubic fit to estimated triple point positions are overlaid on the video. The incident shock can be seen coming in from the left and propagating across the screen with the reflected shock close behind. As the shocks propagate, it is seen that they merge, creating the characteristic "Y" pattern of a Mach stem. The triple point is relatively easy to identify in most of the video, with two exceptions. First, because the camera was hung a short distance above the ground and the backdrop was offset from the propagation line, between $0 < z < 5$ cm the image background is the concrete, with insufficient contrast to extract exact position values for the triple point. Second, beyond $x = 9.14$ m, the shock strength had decreased sufficiently that even with the image processing, estimation of the triple point via visual methods is less trustworthy. In both of these regions, the visual imagery is regarded as supporting evidence for the acoustic data. Additional shock-like shadows can be seen both ahead of and behind the explosion-generated Mach stem and seem to be propagating along the backdrop or along the ground. Whether these are artifacts of the camera focusing, image processing, or physical surface waves has not been determined.

2.4.3 Cross-section

The consistent shock amplitudes from all of the balloon explosions can be compiled to yield one cross-section of the growth of the triple point along the x-z plane, as shown in Figure 10. The blue triangles correspond to microphones that recorded a single shock (Mach stem) while the red

triangles correspond to double shock events (incident and reflected). The green dots correspond to estimates of the triple point position as taken from the high-speed video.

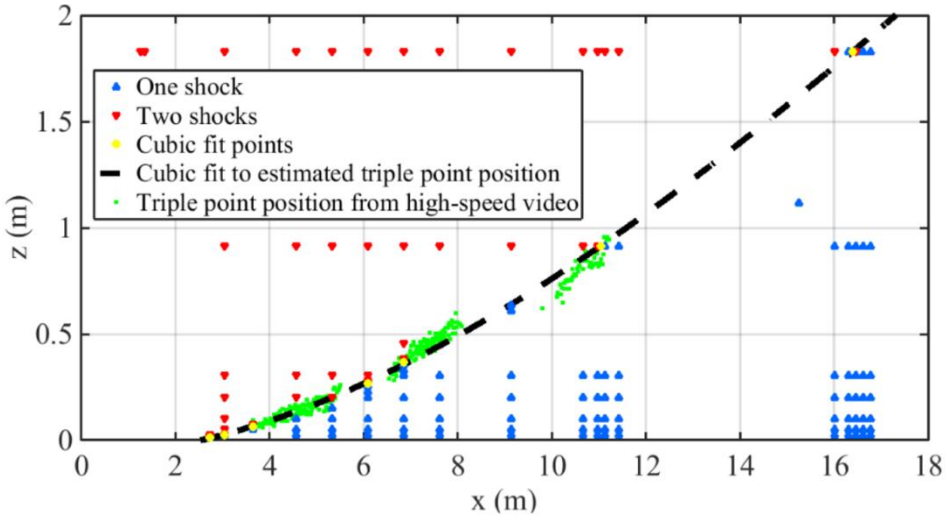

Figure 10 Identification of triple point location for the oxyacetylene explosions, with the red and blue triangles used to identify whether a Mach stem was observed. Green dots represent the position of the triple point extracted from the high-speed footage. The black dashed line is a cubic fit to several points (yellow dots) from the acoustic data where the vertical resolution of the triple point position was within 2.54 cm.

Chapter 3

Comparison to Theory

The results of the experiment from Chapter 2 are now compared to the various theories presented in Chapter 1

3.1 Triple Point Path

In Needham *et al*, standard curves are provided for cubic fits to triple point positions for a 1 kt TNT explosion for several heights of burst. The procedure for scaling one explosion to another is simple, it is assumed that the peak pressure of the shock wave created by an explosion is proportional to the energy released by that explosion, and that the ratio of energy released between two explosions are equal to the cube of the distance ratios of two explosions, or $\frac{P1_{peak}}{P2_{peak}} = \frac{E1}{E2} = \left(\frac{R1}{R2}\right)^3$. If the energy released by an explosion is known in units of kilotons of TNT, then the distances of the equivalent 1 kt of TNT problem can be easily determined.

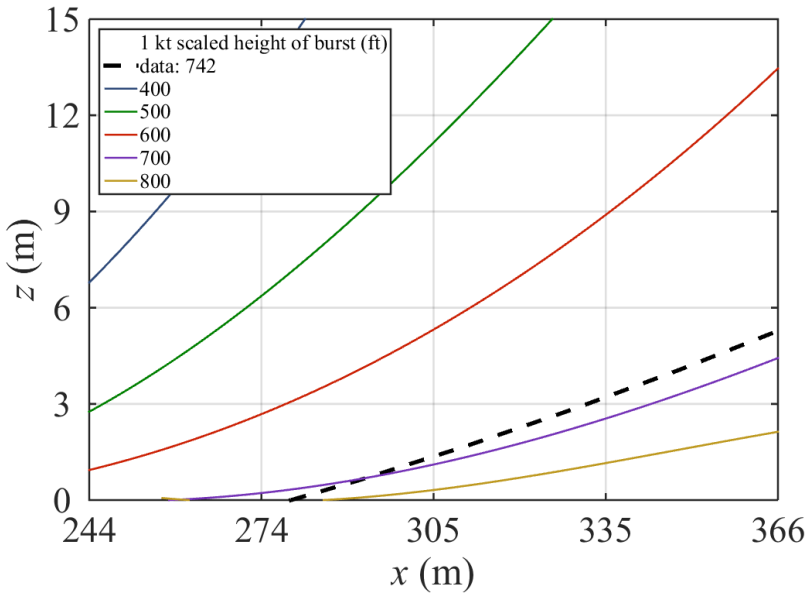

Figure 11 Graph of triple point height as a function of x scaled to explosive yield of 1 kt of TNT. The different colored lines correspond to different heights of burst. Our data (The cubic fit from figure 10) was overlaid

A figure from Ref [11] contains cubic fits for various scaled heights of burst, which is reproduced in part in Figure 11. It also contains the cubit fit for our data superimposed. We can see that our cubic fit starts between two corresponding height of burst curves but it has a distinctively larger slope. This could be a sign that gaseous explosions cannot be scaled exactly the same as high explosives or nuclear blasts. In fact, the ANSI standard for estimating characteristics for a single point explosion in air states that it does not include gaseous explosions in its model heights of burst, even though for solid high explosions it states that 10-20% yield variations between sources is commonplace.

3.2 Transition Point from Regular to Irregular Reflection

The empirical equations from Needham et al. require that we scale our experiment to the equivalent problem of a 1 kt of TNT blast at a certain height of burst (HOB). Equation (3)

corrects an empirical equation given by Needham *et. al.*[11] in cgs units for the distance from the source where the reflection changes from regular to irregular, R_0, for a 1 kt TNT explosion in terms of HOB:

$$R_0 = \left(\frac{170\ \mathrm{HOB}}{1 + 25.05\ \mathrm{HOB}^{0.25}}\right) + (1.7176\ \times 10^{-7})\mathrm{HOB}^{2.5}\,. \tag{3}$$

Substitution of the scaled HOB results in $R_0 = 2.08\ \pm 0.02$ m for our experiment.

To analytically solve for the point of transition from irregular to regular reflection, the value of the parameter a needs to be calculated for each point of reflection along the propagation line. This was done by using the geometry of the experimental setup to find the incident angle of the shock for each point along the propagation line, then, each point along the propagation line was mapped to a peak pressure value of the shock. Using the peak pressure of the shock with the incident angle at each point, the parameter a can subsequently be calculated for each point.

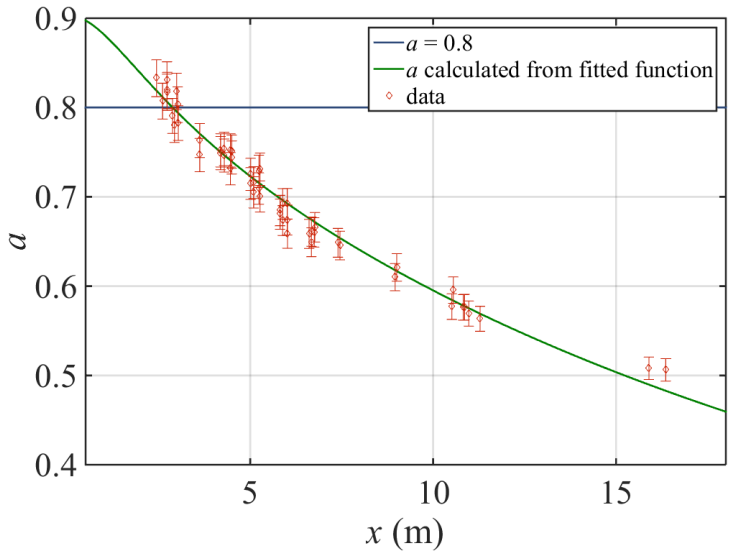

Figure 12 Parameter a vs x. The calculated parameter a for each point along the propagation line. the continuous curve is the derived from the fitted function for P_{sh} while the points correspond the parameter calculated straight from microphone measurements. The error bars are derived from the standard deviation of the peak SPL of the reference microphones to account for variations from the different trials

The green line is the parameter a as calculated from the fitted function, while the red points are the discrete data points. The error bars come from the standard deviation in peak shock pressure from the 25 different trials. The horizontal line corresponds to $a = 0.8$ contour. The derivation in Baskar et al.[9] predicts that the transition from regular to irregular reflection occurs at $a = 0.8$. However, in Karzova *et. al.*[10], which involved weaker shocks than those here, the transition point was experimentally observed to take place at $a = 1.1$.

In our experiment the Mach number and the angle of incidence vary as the shock propagates down the line. The corresponding values of the critical parameter change from $a = 0.9$ at $x = 0$ to $a = 0.46$ at $x = 18$ m. The value of a becomes 0.8 at $x = 2.88 \pm 0.3$ m. The estimated uncertainty stems from applying the peak level variation at the reference probes to the calculation of M_a. It should be noted that the observed transition in Karzova et al., corresponding to $a = 1.1$, is greater than the range of a values obtained in this experiment, signifying that irregular reflection should be present at the ground directly under the explosion, at $x = 0$ m. This is not representative of my results.

3.3 Identification of Irregular Reflection Type

Below is a representative image of the shock a short distance from the explosion. In the close up shock, the discontinuity is shown by highlighting the front of the shock in red. There is a definite angle change at the position of the triple point, indicating that it is probably either a single Mach-Smith reflection or single weak Mach-Smith reflection. A definitive classification would require

that a slipstream exist behind the triple point, but no such thing is seen on the high speed video, however, we doubt that our imaging techniques were sensitive enough to capture such a slipstream even if it existed.

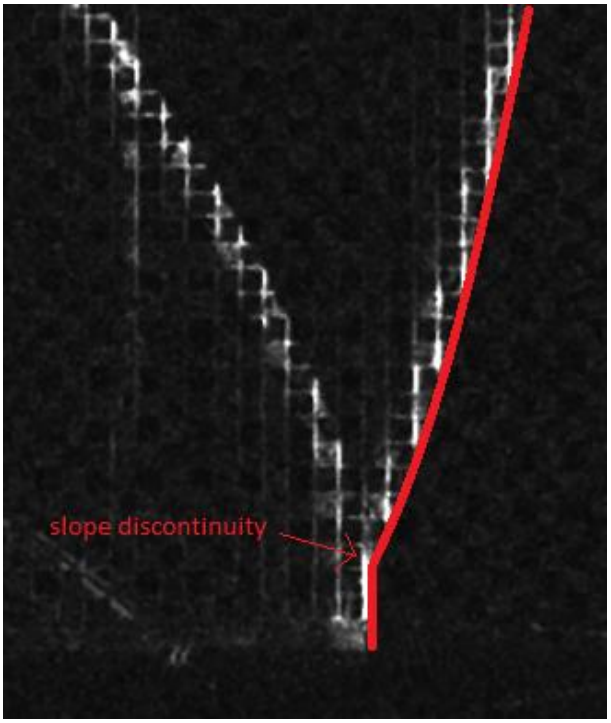

Figure 13 Identification of irregular reflection type. A single frame of the processed high speed video showing the irregular reflection of the shock. The front edge of the incident shock and the Mach stem is highlighted in red to show the slope discontinuity at the triple point. This gives evidence for this reflection to be classified as either a SM-SR or a wSM-SR.

3.4 Summary on the M_s- ϕ Plane

To thoroughly compare these transition criteria and to verify if our shocks indeed fall in the single Mach-smith reflection regime, all are overlaid on this updated version of the M_s- ϕ plane.

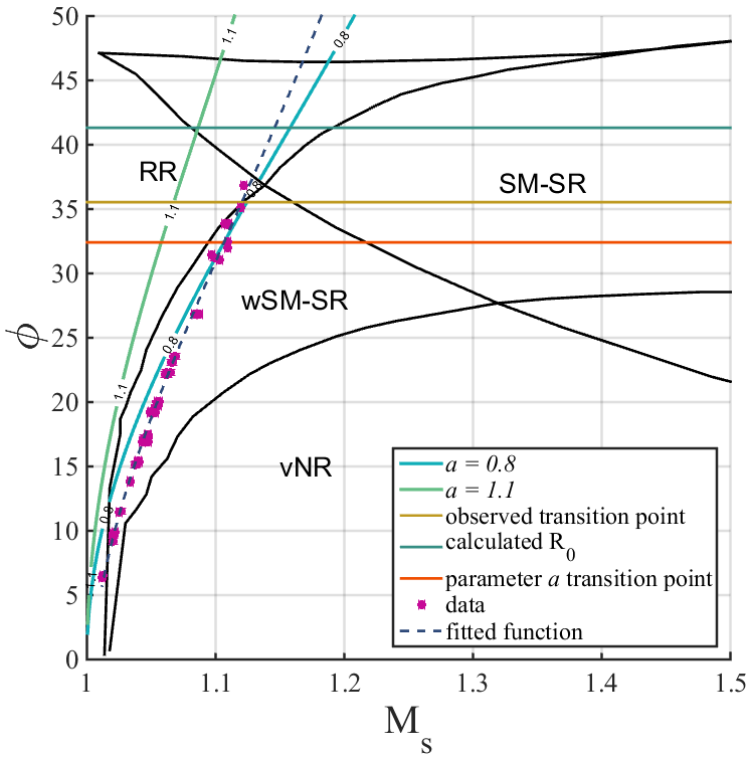

Figure 14 $\boldsymbol{\phi}$-$\boldsymbol{M_s}$parameter space revisited. Shown is a graph of the $\boldsymbol{\phi}$-$\boldsymbol{M_s}$parameter space with the transition criteria from Semenov *et al*., the parameter $\boldsymbol{a}$ contours, the trace of our explosion data along the propagation line, and three horizontal lines corresponding to the $\boldsymbol{x}$-values of the transition point from the r0 and parameter $\boldsymbol{a}$ calculations and our observed transition point.

The observed transition point for irregular reflections is similar, but falls between, the locations predicted for lower amplitude sources and the empirical formulas from large explosive yields. The Baskar *et al.* analytical value $a = 0.8$ overestimates the observed transition point, while the R_0 from large scale explosions underestimates it. The details of the derivation of the critical parameter provide a clue as to a possible explanation for the overestimation. In Baskar et al., a was derived for the transition from regular to the von Neumann reflection. However, the reflections observed in this experiment can be seen in the high-speed video to have a slope discontinuity at the intersection of the Mach stem and the incident wave, which characterizes a single Mach reflection.

The triangular region between 47 and 35 degrees is labeled in Semenov *et. al.* as region that has been "completely ignored" by research. Though no actual data points of ours were located in this region (because the array of pressure microphones would have been over saturated) the fitted function for the acoustic overpressure would suggest that our experiment traces right through it. It would suggest that this regime could be classified as a regular reflection. However, the high speed imaging is very unclear at this point, so exact classification is inconclusive. The transition point from irregular reflection is from regular reflection to SM-SR, which is consistent with our observations.

3.5 Concluding Discussion

We have observed, through both acoustic data and high-speed video imaging, the transition from regular to irregular reflection of shock waves and Mach stem growth in a regime not previously studied. Although the high-speed video effort was limited by the preliminary nature of our experiment, it provides sufficient evidence to verify the acoustical methods used to localize the triple point position. A previous empirical estimate, derived from explosions several orders of magnitudes greater, underestimate the observed transition point. Conversely, estimates based on an analytical solution, derived for weaker shocks in a regime for von Neumann reflections, overestimates the transition point. However, the method of tracing the shock reflection directly on the M_s and ϕ parameter space agrees very well with observations, showing that this explosion does agree with traditional three shock theory.

3.7 Acknowledgements

The authors are grateful to the BYU Office of Research and Creative Activities for Undergraduate Research and Mentoring Environment Grants. We are also grateful to Drs. Gabi Ben-dor, Charles Needham, David Blackstock, Maria Karzova, and Jeffrey Macedone for their helpful communications.

Index

Works Cited

[1] E. Mach, “Uber den Verlauf Von Funkenwellen in der Ebene und im Raume”, Sitzungsbr. Akad. Wiss. Wein 78, 819-838 (1878)
[2] J. Von Neumann, “Oblique reflection of shocks,” in John von Neumann Collected Work, edited by A. H. Taub (MacMillan, New York, 1963), Vol. 6, pp. 238-299
[3] P. Colella and L. F. Henderson, “The von Neumann paradox for the diffraction of weak shock waves, J. Fluid Mech. 213, 71–94 (1990).
[4] G. Ben-Dor, Shock Wave Reflection Phenomena (Springer Verlag, New York, 2007), pp. 3-4, 297-303
[5] E. I. Vasiliev and A. N. Kraiko, “Numerical simulation of weak shock diffraction over a wedge under the von Neumann paradox conditions.” Comput. Math. Phys. 39, 1335-1345 (1999)
[6] B. Skews and J. Ashworth, “The physical nature of weak shock wave reflection,” J. Fluid Mech. 542, 105-114 (2005).
[7] A.N. Semenov, M.K. Berezkina, I.V. Krassovskaya, “Classification of pseudo-steady shock wave reflection types”, Shock Waves, 22, 307-316 (2012).
[8] M. Geva, O. Ram. and O. Sardot, “The non-stationary hysteresis phenomenon in shock wave reflections”, J.Fluid Mech. 732 R1 (2013)
[9] S. Baskar, F. Coulouvrat, and R. Marchiano, “Nonlinear reflection of grazing acoustic shock waves: Unsteady transition from von Neumann to Mach to Snell-Descartes reflections,” J. Fluid Mech. 575, 27-55 (2005)
[10] M. M. Karzova, V. A. Khokhlova, E. Salze, S. Ollivier, and P. Blanc-Benon, “Mach stem formation in reflection and focusing of weak shock acoustic pulses,” J. Acoust. Soc. Am. 137, EL436 (2015)
[11] C. E. Needham, Blast Waves (Springer, New York, 2010), pp. 216-217,
[12] ANSI S2.20-1983, “American National Standard for estimating airblast characteristics for single point explosions in air,” (Acoust. Soc. Am., New York, 2006)
[13] M. B. Muhlestein, K. L. Gee, and J. H. Macedone, “Educational demonstration of a spherically propagating acoustic shock,” J. Acoust. Soc. Am. 131, 2422-2430
[14] S. M. Young, K. L. Gee, T. B. Neilsen, K. M. Leete, “Outdoor measurements of spherical acoustic shock decay”, J. Acoust. Soc. Am., submitted, minor revisions completed (2015).